ELSEVIER

Journal of Electron Spectroscopy and Related Phenomena 88–91 (1998) 171–177

JOURNAL OF ELECTRON SPECTROSCOPY and Related Phenomena

Invited paper

Spin polarized photoemission from amorphous alloy surfaces

J.A.D. Matthew[a,*], E.A. Seddon[b], Y.B.O Xu[c]

[a]*Department of Physics, University of York, Heslington, York YO1 5DD, UK*
[b]*Daresbury Laboratory, Warrington, Cheshire WA4 4AD, UK*
[c]*Department of Physics, The University of Leeds, Leeds LS2 9JT, UK*

Abstract

Recent results on spin polarized photoemission and photon excited secondary electron emission from the surfaces of ferromagnetic amorphous alloys Fe–B, Co–B and Fe–Y are reviewed. Spin resolved density of states calculations suggest that the spin polarization profile is very sensitive to the theoretical model chosen, but experiments demonstrate that the spin up density dominates at the Fermi edge in the iron-based alloys, while the spin down density is greater in the cobalt alloy. Variation of photon energy from 15–110 eV allows polarization of sp states to be probed as well as d states and evidence for contributions to the magnetic moment from Y in $Fe_{60}Y_{40}$ and B in $Co_{77}B_{23}$ are examined. Photon excited secondary electrons provide a flexible monitor of surface magnetization: relative contributions to the polarization from spin polarization in the conduction band and spin dependence of the mean free path are separated by studying the variation of electron polarization with the kinetic energy of emission. © 1998 Elsevier Science B.V.

Keywords: Amorphous alloy surfaces; Polarization and emission; Spin polarized photoemission

1. Introduction

Amorphous alloys have a number of large-scale commercial applications, the most important of which spring from their 'soft' magnetic properties. For example, as wear-resistant thin films they find use in tape recorder heads, as strips they are the basis of electronic article surveillance tags [1] and wound into toroids they find use in compact power supplies. In the USA and Japan in particular, they are also widely used in the cores of the ubiquitous local area distribution transformers.

Most 'standard' metallic samples exhibit a degree of crystallinity, which means that the constituent atoms are, more-or-less, ordered. In contrast to this, amorphous metals are prepared by techniques that are designed to ensure a breakdown in the long-range order, such as melt spinning or sputtering, and as a result of this their properties are often strikingly different from those of their crystalline counterparts.

A fundamental parameter relevant to the study of magnetic materials is the net spin density of the valence electrons and any technique that can provide insight into this is an important probe of magnetism. This is especially true for transition metal systems for which any magnetism due to the orbital moments is largely quenched and thus the magnetism, M, is proportional to $n_{\uparrow} - n_{\downarrow}$, where $n_{\uparrow(\downarrow)}$ represents the number of electrons in the conduction band with spin up(down). In spin polarized photoemission the polarization, P, of an energy selected photoemitted beam is determined. P is the difference signal for the two spin orientations divided by their sum

* Corresponding author. Tel: 00 44 1904 432253; e-mail mmg@ohm.york.ac.uk.

PII S0368-2048(97)00109-6

ie $[N_\uparrow - N_\downarrow]/[N_\uparrow + N_\downarrow]$ where $N_{\uparrow(\downarrow)}$ is the number of spin up(down) electrons emitted. As $N_{\uparrow(\downarrow)}$ may be closely related to $n_{\uparrow(\downarrow)}$ there is a direct connection between P and M.

This paper reviews the prediction of recent self consistent theoretical calculations of the spin resolved densities of states of amorphous magnetic alloys [2,3] with experimental spin resolved photoemission results obtained on the spin polarized photoemission facilities at the Daresbury Laboratory [4–6]. The systems considered are $Fe_{80}B_{20}$ and $Co_{77}B_{23}$, prototypes of the technologically important magnetic alloys, and $Fe_{60}Y_{40}$ which shows a rich variety of magnetic behaviour.

2. Experiment

Daresbury Laboratory routinely operates two polarimeters on stations of the SRS. The first a conventional high-energy (100 kV) Mott polarimeter [7]. The second a compact, lower scattering voltage (20 kV) retarding potential polarimeter; both have been described in detail elsewhere [8,9]. The latter polarimeter facility, in particular, incorporates a number of advantageous features.

1. The polarimeter has four channel plate detectors rather than the more usual channeltrons. This has led to a compact device that is capable of simultaneously resolving two components of an electron beam polarization without sacrificing spin sensitivity.
2. The polarimeter is mounted at the exit to a hemispherical energy analyser that offers good energy resolution and which itself is mounted on a two-circle goniometer. The whole apparatus can then be used on a range of stations of the SRS: flexibility that means that experiments over a wide range of photon energies and photon polarizations are, in principle, possible.
3. The apparatus is also consistent with a range of standard sample handling and cooling options, including both liquid N_2 and liquid He cooling.

In making a comparison between theory and experiment it is important to understand what is actually measured: in the experimental arrangement of Fig. 1 the sample is magnetized in the horizontal

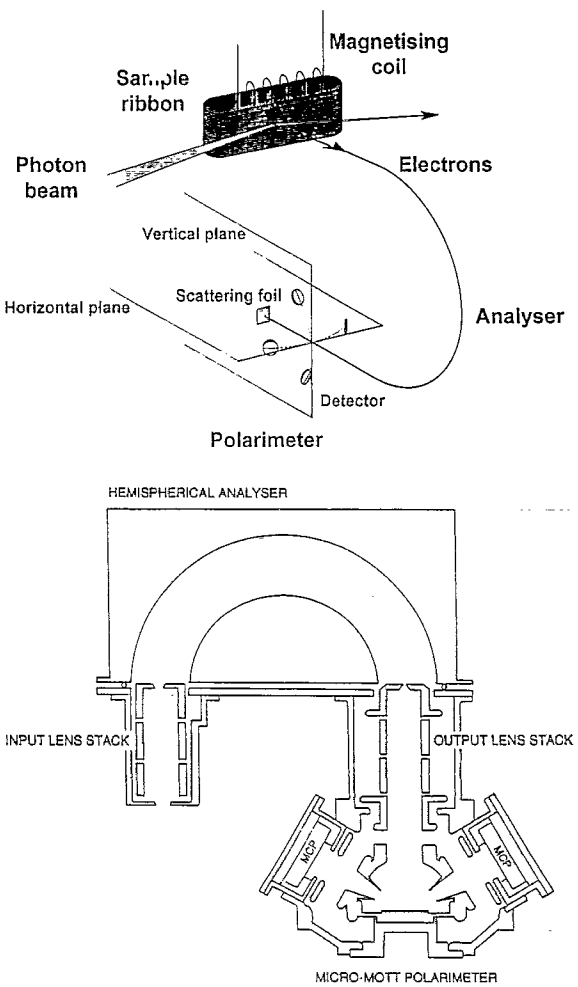

Fig. 1. Schematic diagram of the Daresbury spin detection system.

direction leading to the emission of photoelectrons with a net spin bias also in the horizontal direction. Through the $L.S$ spin orbit interaction with the Au atoms in the Mott polarimeter there is then an associated asymmetry in the signals of the two *vertical* detectors, but no asymmetry in the *horizontal* signals. The vertical signals are then processed to give $P = (N_\uparrow - N_\downarrow)/(N_\uparrow + N_\downarrow)$ as in Fig. 2: the measured P may then be combined with a conventional spin averaged photoemission signal to give the spin up and spin down emission profiles that are related to (but not necessarily equal to) the spin resolved densities of states calculated by the theoreticians. Measuring P is not easy: maxima in P may occur when $N_\uparrow + N_\downarrow$ is small, but $N_\uparrow - N_\downarrow$ comparable, i.e. associated

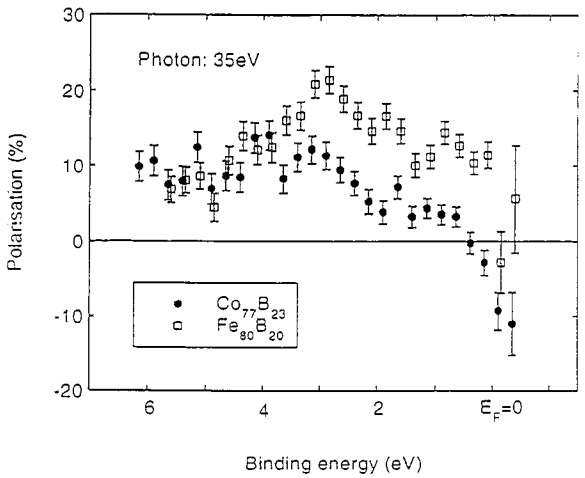

Fig. 2. Comparison of the spin polarization of $Fe_{80}B_{20}$ and $Co_{77}B_{23}$ for a photon energy $h\nu$ = 35e V [5].

with near minima in the respective densities of states. Long-term detector stability coupled with the requirement of high statistical precision are then needed to give reliable spin resolved photoemission profiles. The Daresbury facilities have been demonstrated to satisfy these demands.

The flexibility in photon energy that synchrotron sources provide is important in obtaining good spin polarized results for a number of reasons. At high photon energies the cross-sections for conduction band photoemission are very low (although See and Klebanoff [10] have successfully used Mg Kα radiation to obtain such data): at photon energies of 50–100 eV photoemission becomes strongly surface sensitive and comparison with bulk state densities becomes doubtful. For $h\nu \geq 30$ eV the Fe 3d cross-section dominates those of B or Y [11] so that the spin resolved experiment essentially probes the Fe 3d spin resolved partial densities of states of the materials. For these reasons photon energies of $h\nu$ = 35 eV and 110 eV were chosen for the majority of the Daresbury experiments, though some investigations at very low photon energies ($\sim$15 eV) have been carried out to probe moments on elements other than Fe.

The true secondary electrons (conveniently studied in the electron kinetic energy range 1–20 eV) also exhibit spin polarization and have the bonus that they are much more plentiful than the conduction band photoemission. At the higher energy (20–30 eV) theory [12] implies that P is closely related to $(n_\uparrow - n_\downarrow)/(n_\uparrow + n_\downarrow)$, where here $n_{\uparrow(\downarrow)}$ denotes the *total* electron content of the spin up(down) conduction band.

In the studies reviewed here the samples of $Fe_{80}B_{20}$ and $Co_{77}B_{23}$ were prepared by melt spinning in a He or Ar atmosphere and then cleaned in situ by argon ion bombardment [5,6]. Compositions were checked by in-situ Auger electron spectroscopy and by XPS on the RUSTI Scienta spectrometer at the Daresbury Laboratory. The amorphous character of the ribbons was confirmed by X-ray diffraction both before and after experiment. $Fe_{60}Y_{40}$ samples were in situ magnetron sputtered on an amorphous alloy substrate ($Co_{77}B_{23}$) already formed in a closed loop with an associated magnetizing coil [7]: these conditions have been shown to produce amorphous films in the metal composition range 0.32–0.88 [13]. By varying the current in the magnetizing coil and observing the low-energy secondary electron emission hysteresis loops may be readily obtained. At room temperature, $Fe_{80}B_{20}$ and $Co_{77}B_{23}$ were consistently ferromagnetic for all compositions achieved—see Fig. 3. In contrast, Fe_xY_{100-x} showed no hysteresis at room temperature, but on lowering the temperature to 114 K $Fe_{60}Y_{40}$ became ferromagnetic, while $Fe_{40}Y_{60}$ remained paramagnetic.

3. Theory

The last 10 years has seen great progress in understanding the ground state electronic properties of complex materials through the application of self consistent quantum mechanical formalisms within the local density approximation. Understanding amorphous magnetic alloys requires two important extensions of conventional methods. Firstly, spin polarized electronic structure calculations are required and secondly the amorphous environment has to be simulated by incorporating appropriate short-range order within a supercell which is large enough for the artificially imposed long-range periodicity to have little effect. This may be achieved by using molecular dynamics within a hybridized nearly free electron tight binding approach [3]: such simplified interatomic potential models can be solved for very large unit cells (>1000 atoms), but the basic pattern that emerges may be incorporated into a smaller supercell

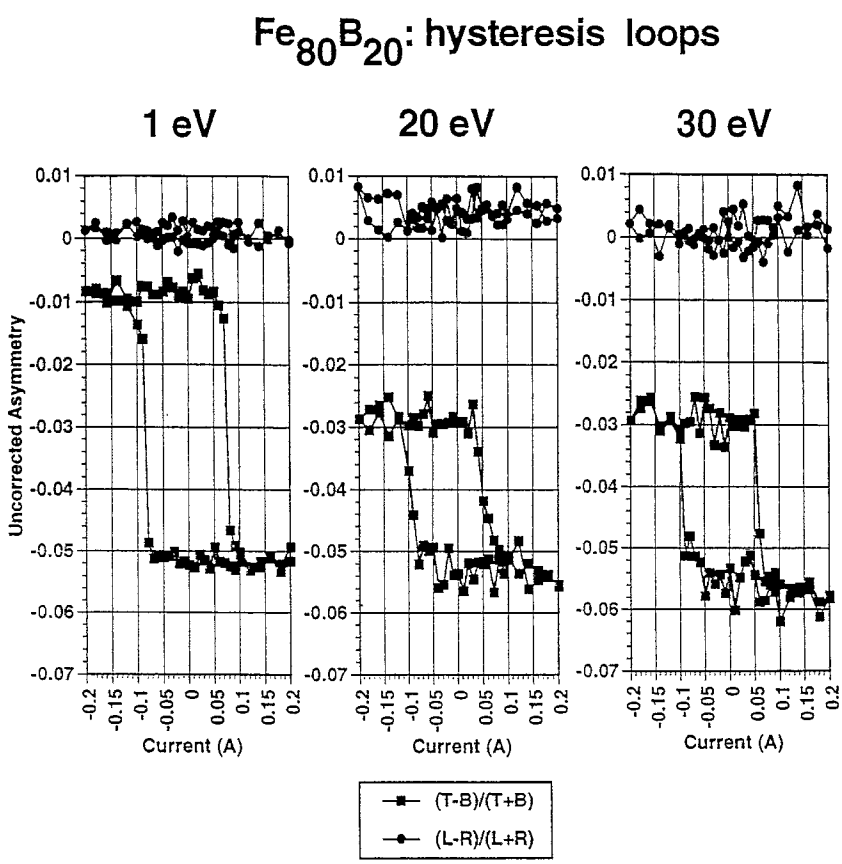

Fig. 3. The spin polarized detection system operated as a surface magnetometer: hysteresis loops for $Fe_{80}B_{20}$ at secondary electron energies 1, 20 and 30 eV. The left and right detectors (L and R) show no asymmetry on average, while the top and bottom detectors follow the near surface magnetisation ($\propto$ (T − B)/(T + B)).

(~60–70 atoms) upon which a self-consistent electronic structure calculations can be carried out. Self-consistency with spin polarization in cells of such size still poses problems and early calculations achieved self-consistency for an 'average atom' in the cell [14] or limited self consistency *between* the exchange splitting and the magnetic moment within a Hubbard Hamiltonian [15]. Recently Hafner et al. [2,3] achieved full local self consistency in a linearized–muffin–tin–orbital (LMTO) supercell model, which gives similar average magnetic moments to previous methods, but for Fe_xB_{100-x} demonstrated the appearance of negative Fe moments at low B concentration.

For Fe rich Fe_xB_{100-x} the recent theoretical methods are in broad agreement as exemplified by the spin resolved densities of states for $Fe_{80}B_{20}$ calculated by Hafner et al. [2]—Fig. 4. In the 8–10 eV binding energy region (not shown) there is a non bonding non spin polarized B 2s band in both the majority- and minority-spin channels, ie no net spin polarization. At lower binding energy hybridized Fe 3d/B 2p states show strong spin dependence. In the majority-spin band, the two prominent peaks are reminiscent of the e_g/t_{2g} splitting in crystalline bcc Fe. The relatively high coordination in the amorphous environment leads to similar, though broadened, peaks. Crudely, the minority-band is shifted relative to the majority-band so that only the lower of the 'e_g/t_{2g}' peaks is fully occupied. At a more quantitative level, the theoretical predictions are highly model dependent and spin resolved photoemission can potentially resolve these differences. Co_xB_{100-x} exhibits a similar pattern with important differences that will emerge in the comparison with the photoemission data.

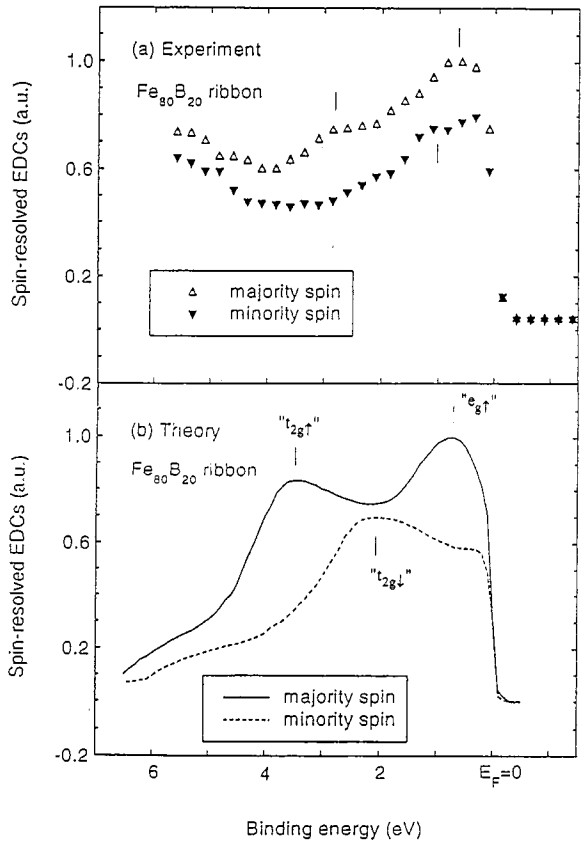

Fig. 4. (a) Experimental spin resolved electron energy distribution (EDC) curves of amorphous $Fe_{80}B_{20}$ [5]. (b) Theoretical spin resolved bulk density of states by Hafner *et al.* [2], broadened to take account of the experimental energy resolution.

In the case of Fe_xY_{100-x} [3] there is strong evidence of ferrimagnetic character and at Y concentrations >30% the relationship between the spin resolved density of states and that of Fe is much less clear (Fig. 5). However, the level of agreement between theory and experiment will be very sensitive to the structural integrity of the methods as in this system there is a tendency to form Fe clusters at high Y levels—the extent to which this occurs will strongly influence the spin polarization profile.

4. Comparison of theory and experiment

Fig. 4 compares the experimentally determined spin resolved photoemission energy distribution curve of $Fe_{20}B_{80}$ for photon energy $h\nu$ = 35 eV with the calculation by Hafner et al. [2] of the occupied bulk Fe 3d partial density of states broadened to take account of the finite energy resolution (~0.2 eV) of the photoemission experiment. Since the degree of hybridization with B 2p states is consistent throughout this region the total spin resolved density of states is very similar to the partial state density, but the photoionization cross-section at $h\nu$ = 35 eV is Fe3d dominated [11]. As noted previously, the theoretical majority-spin band show '$e_{g\uparrow}$' and '$t_{2g\uparrow}$' like features, while in the minority-band only the '$e_{g\downarrow}$' are filled with '$t_{2g\downarrow}$' occupation just commencing. The experimental spin resolved EDCs show a similar pattern, although the high binding energy feature is less prominent than in the theory. This is a well known matrix element effect in which the transition rate increases by a factor of ~2 between the bottom and top of the d-band in this photon energy regime [16]. The splitting between the peaks is smaller than in the theory and '$t_{2g\downarrow}$'-like peak is prominent at slightly smaller binding energy than in the theory. The experimental EDCs are very similar at 35 and 110 eV and are also similar to those of polycrstalline Fe [6]. As shown in Fig. 4, the majority-spin states have higher density than the minority-spins at the Fermi edge, a result consistent with the theoretical predictions of Hafner et al., but contrary to the earlier work of Nowak et al. [14] and Bratkovsky and Smirnov [15].

$Co_{77}B_{23}$ is similar in profile, but with an important difference—the minority-carriers are now in the ascendancy at the Fermi edge as shown in the polarization measurements in Fig. 2. The additional d electron leads to further filling of the minority-band with the second majority-peak being pushed away from the Fermi edge [16]. This effect can also be observed in the X-ray photoemission studies of See and Klebanoff [10], but is more clearly resolved in this soft X-ray study.

In $Fe_{57}Y_{43}$, theory predicts that single broad peaks dominate both the majority- and minority-spin bands with the majority-band shifted well below the Fermi level so that the minority-density predominates at the Fermi edge. This is contrary to our experimental observations ($h\nu$ = 110 ev), namely a pattern not dissimilar to polycrystalline Fe, but with lower net polarization. This is probably due to the tendency of Y and Fe atoms to segregate at higher Y concentrations, a phenomenon indicated by the molecular dynamics

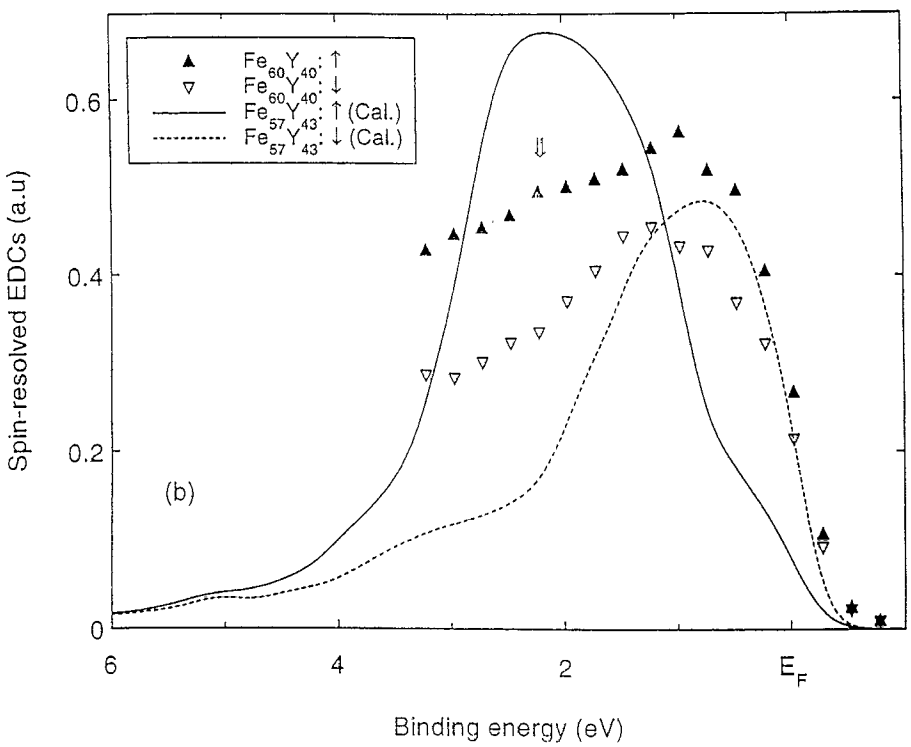

Fig. 5. Experimental spin resolved EDC curves of $Fe_{60}Y_{40}$ [6] compared with theoretical spin resolved bulk densities of states of $Fe_{57}Y_{43}$ of Becker and Hafner [3], broadened to take account of experimental energy resolution.

calculations of Becker and Hafner [3] and further suggested by conventional photemission on Fe_xY_{100-x} alloys ($h\nu = 40.8$ eV) by Cossy–Favre et al. [17]. The 64-atom unit cell used in the fully self-consistent electronic structure calculations was insufficient to model this segregation behaviour, but qualitatively the effect is likely to drive the polarization towards elemental metal behaviour with the lower asymmetry partly associated with the disordered superparamagnetic moments of Fe-rich clusters, as suggested by Coey et al. [18].

At a photon energy of $h\nu = 110$ eV the Y cross-section is close to its Cooper minimum [11] and so the experiments are monitoring Fe moments and carry no information about possible ferrimagnetic behaviour with oppositely oriented Y moments. In the systems discussed here, it would be helpful to probe the magnetic behaviour of the atomic species complementing the transition metal (B or Y). This can be approached in two ways, either by variation of photon energy or by studying polarization of the true secondaries. In Fe_xB_{100-x} and Co_xB_{100-x} the B 2p cross-section becomes comparable with Co and Fe 3d cross-sections at $h\nu \sim 15$ eV [11]: preliminary experiments under these conditions reveal a different polarization pattern from that obtained in experiments at $h\nu = 35$ eV and 110 eV with a distinct dip in P at binding energies around 2 eV. Whether this can be interpreted as photoemission contributions of B atoms with no moment or with B moments opposite to that of Fe is currently under investigation.

It is not possible to find a photon energy regime where the Y cross-section is as great as that of Fe, but there is some evidence of ferrimagnetic behaviour in the secondary electron spin polarization of $F_{60}Y_{40}$. Following the ideas of Penn et al. [12] the secondary electron polarization at $E \sim 20$ eV corresponds to the average spin polarization in the conduction band, while at lower electron energy the spin asymmetry becomes greater than the conduction band polarization due to the spin dependence of the mean free paths of the emitted electrons. This is just the behaviour observed in $Fe_{80}B_{20}$ (Fig. 3). However, $F_{60}Y_{40}$ has

an anomalously low secondary electron polarization (7% at 1 eV) compared with a conduction band polarization of 14%. The conduction band photoemission is probing only the Fe 3d moments, while the secondary electron emission may be more representative of all the moments in the system. Further experiments examining systematic trends in P with composition and secondary electron energy are in progress.

5. Conclusions

Recent theories of the spin resolved densities of states of amorphous Fe_xB_{100-x}, Co_xB_{100-x} and Fe_xY_{100-x} are shown to be in reasonable accord with spin-polarized photoemission data. In the borides correct spin densities at the Fermi edge are predicted, while in Fe_xY_{100-x} evidence of clustering of Fe and Y atoms is revealed. Future developments in synchrotron sources and spin polarimeters will open the way for spin polarized electron emission to become a more routine monitor of surface magnetism.

Acknowledgements

The authors wish to thank D. Greig, A.L. Mitchell, M. Dowling, C.G.H. Walker, P.K. Hucknall and K. Donovan for contributions to the experimental programme, J. Turton and P. Hector for skilled technical help and D. Teehan for synchrotron support. The work was funded by EPSRC UK and X.B. Xu acknowledges support from ORS and the University of Leeds.

References

[1] J. Ryan Jr., Working Knowledge, Scientific American, May 1997, p. 92.
[2] J. Hafner, M. Tegze, Ch. Becker, Phys. Rev. B 49 (1994) 285.
[3] Ch. Becker, J. Hafner, Phys. Rev. B 50 (1994) 3913.
[4] Y.B. Xu, C.G.H. Walker, D. Greig, E.A. Seddon, I.W. Kirkman, F.M. Quinn, J.A.D. Matthew, J. Phys. Condens. Matter 8 (1996) 1567.
[5] Y.B. Xu, D. Greig, A.L. Mitchell, E.A. Seddon, J.A.D. Matthew, J. App. Phys. 81 (1996) 4419.
[6] Y.B. Xu, D. Greig, E.A. Seddon, J.A.D. Matthew, Phys. Rev. B 55 (1996) 11442.
[7] N.F. Mott, Proc. Soc. Lond. Ser. A 124 (1929) 425.
[8] F.M. Quinn, E.A. Seddon, I.W. Kirkman, Rev. Sci. Instrum. 66 (1995) 1564.
[9] E.A. Seddon, I.W. Kirkman, F.M. Quinn, in: H. Kleinpopper, R. Newall (Eds.), Polarized Electron/Polarized Physics, Plenum, New York, 1995, p. 95.
[10] A.K. See, L.E. Klebanoff, J. Appl. Phys. 79 (1996) 4796.
[11] J.J. Yeh, I. Lindau, Atom. Data Nucl. Data Tables 32 (1985) 1.
[12] D.R. Penn, S.P. Apell, S.M. Girvin, Phys. Rev. 32 (1985) 7753.
[13] J.M.D. Coey, D. Givord, A. Liénard, J.P. Rebouillat, J. Phys. F 11 (1981) 2707.
[14] H.J. Nowak, O.K. Andersen, T. Fujiwara, O. Jepson, P. Vargas, Phys. Rev. B 44 (1991) 3577.
[15] A.M. Bratkovsky, A.V. Smirnov, J. Phys. Condens. Matter 5 (1993) 3203.
[16] H. Tanaka, S. Takayama, M. Hasegawa, T. Fukunaga, U. Mizutani, A. Fujita, K. Fukamichi, Phys. Rev. B 47 (1993) 2671.
[17] A. Cossy-Favre, H.-G. Boyen, O. Oelhafen, Ch. Becker, J. Hafner, J. Non-Crystalline Solids 205-207 (1996) 587.
[18] J.M.D. Coey, J. Appl. Phys. 49 (1978) 1646.